

The Unique Carrier Mobility of Janus MoSSe/GaN Heterostructures

Wen-Jin Yin¹, Xiao-Long Zeng¹, Bo Wen², Qing-Xia Ge¹, Ying Xu¹, Gilberto Teobaldi^{3,4,5}, and Li-Min Liu^{*2}

¹*School of Physics and Electronic Science, Hunan University of Science and Technology, Xiangtan 411201, China*

²*School of Physics, Beihang University, Beijing 100083, China*

³*Scientific Computing Department, STFC UKRI, Rutherford Appleton Laboratory, Harwell Campus, OX11 0QX Didcot, United Kingdom*

⁴*Stephenson Institute for Renewable Energy, Department of Chemistry, University of Liverpool, L69 3BX Liverpool, United Kingdom*

⁵*School of Chemistry, University of Southampton, Highfield, SO17 1BJ Southampton, United Kingdom*

Corresponding authors: liminliu@buaa.edu.cn

Abstract

Heterostructure is an effective approach in modulating the physical and chemical behavior of materials. Here, the first-principles calculations are conducted to explore the structural, electronic, and carrier mobility properties of Janus MoSSe/GaN heterostructures. This heterostructure exhibits a superior high carrier mobility of $281.28 \text{ cm}^2\text{V}^{-1}\text{s}^{-1}$ for electron carrier and $3951.2 \text{ cm}^2\text{V}^{-1}\text{s}^{-1}$ for hole carrier. Particularly, the magnitude of the carrier mobility can be further regulated by Janus structure and stacking modes for the heterostructure. We reveal that the equivalent mass and elastic moduli strongly affect the carrier mobility of the heterostructure, while the deformation potential contribute the different carrier mobility for electron and hole of the heterostructure. These results suggested that the Janus MoSSe/GaN heterostructure has many potential applications for the unique carrier mobility.

Introduction

The increasing development of technology triggers the revolution of electronic device or vehicle toward microminiaturization and multifunctional.^[1-3] It is well known that size and intrinsic property of a material are the two crucial factors. That means it should be in nanocrystalline, as well as own with desirable band gap and carrier mobility. The successful exfoliation of graphene shines the light on the potential of low dimensional material production. Meanwhile, it shows that graphene exhibits half-integer quantum hall effect, high migration rate, and mass less carrier transport properties;^[4,5] However, the absence of band gap in pristine sheet leads to an extremely low on/off ratio, which severely limits its further application in nanoscale electronic device.^[6-8] Thus, it has aroused extensive attention to modulate the electronic structure.

Structure tailoring is a common method to control the electronic property, such as forming armchair or zigzag edge nanoribbons. Although a small band gap can be open, the carrier mobility would be dramatically reduced due to the missing of Dirac cone and scattering effect in the nanoribbons.^[9,10] For example, sub-10 nm nanoribbon field

effect transistors shows that the carrier mobility dropped to less than $200 \text{ cm}^2\text{V}^{-1}\text{s}^{-1}$ with diminishing width when the enough band gap opened.^[11] On the other hand, introducing defect, doping, or surface modification can also regulate the electronic property of a material. But it is totally unavoidable to bring foreign atom into the system, where it will often serve as an electron or hole carrier trap site.

Apart from above approaches, searching for graphene analogue is fascinating, and shows strong vitality.^[12, 13]^[14] Transition metal dichalcogenides (TMDs) have received great interests. Through varying the collocation of chalcogen S, Se, and Te atoms and transition metal Mo, W, Nb and V atoms, plenty of TMDs structures with tunable band gaps can be obtained.^[15, 16] Single layer MoS_2 , as a typical member of TMDs family, is a semiconductor with a band gap of about 1.9 eV ,^[17] and it has been regarded as a promising candidate for field effect transistor with an on/off ratio exceeding 10^8 .^[18] However, the previous result clearly shows that carrier mobility of a suspended MoS_2 sheet is found to be in the range of $0.5\text{-}3 \text{ cm}^2\text{V}^{-1}\text{s}^{-1}$, thus this small mobility will cause low efficiency for the electronic devices.^[19-21] Further work showed that through removing adsorbates or depositing atop a high-dielectric layer, extrinsic scatters can be partially suppressed, and the value of carrier mobility can be increased to $200 \text{ cm}^2\text{V}^{-1}\text{s}^{-1}$.^[22-25] In addition, the magnitude of carrier mobility can also be remained in its armchair nanoribbons.^[26]

Recently, a new kind of TMDs named Janus MoSSe has been reported,^[27] where it obtained through breaking the out-of-plane structural symmetry of MoS_2 .^[28, 29] Superior to the MoS_2 ,^[30-32] an intrinsic dipole exists in the vertical direction of the Janus sheet,^[33, 34] and theoretical result shows that the carrier mobility of single layer is about $157 \text{ cm}^2\text{V}^{-1}\text{s}^{-1}$ for hole carrier and $74 \text{ cm}^2\text{V}^{-1}\text{s}^{-1}$ for electron carrier. The carrier mobility can be further adjusted by varying the thickness like forming double or triple layers as homo heterostructure with the electron carrier at $1194 \text{ cm}^2\text{V}^{-1}\text{s}^{-1}$ and hole carrier at $5894 \text{ cm}^2\text{V}^{-1}\text{s}^{-1}$ predicted by theoretical calculations.^[33] Inspired by this, it is interesting to know the effect of heterostructure.^[35] Because heterostructure can not only preserve the property of its individual component, but also introduce advanced functional.^[36-38] For example, the heterostructure of the different semiconductors could exhibit unusual band gap.^[39, 40] What's more, intrinsic electric field may generally exist in the heterostructure, and it would help to separate the carriers.^[41-43] Meanwhile, Schottky barrier in the heterostructure^[44] can also effectively reduce the recombination of electron-hole pairs and improve the life time of the carriers.^[45] The formation of heterostructure requires the two components, owing some familiar behaviors. Luckily, the recent advancements in 2D group III-V compounds with simple wurtzite or zinc-blende structures like nitride GaN brings hope to further improve the single layer TMDs. The electronic band gap of single layer GaN can vary from 1.9 eV to 3.0 eV for different configurations.^[46] The lattice parameters of GaN are quite similar to single layer TMDs.^[47] And it has been reported that the formation of heterostructure with internal polarization can effectively reduce the band gap.^[48] Thus, it is interesting to know the carrier behavior of the heterostructure between single layer Janus TMDs and nitride GaN.

In this work, we aim to unveil the structural and electronic properties of the Janus MoSSe/GaN heterostructure by the first-principles calculations. The outline of the paper can be organized as the following: Firstly, we systematically study the stabilities of the MoSSe/GaN heterostructures. Then, we examine the carrier mobility and the electronic behavior of the heterostructures. At last, the crucial factors on determining carrier mobility behavior will be discussed.

Computational Method

All simulations were carried out at Density Functional Theory (DFT) level as implemented in the Vienna ab initio simulation program package (VASP),^[49, 50] with the Perdew-Burke-Ernzerhof (PBE) exchange-correlation functional under the generalized gradient approximation (GGA).^[51] The projector augmented wave (PAW) method was used to represent the electronic density at the atomic cores. The plane-wave energy cutoff was 500 eV, checked to be sufficiently accurate against calculations with higher cutoffs. The convergence criterion for the self-consistency procedure was 10^{-6} eV. We used a $15 \times 15 \times 1$ Monkhorst-Pack \mathbf{k} -point grid in the Brillouin zone, with one \mathbf{k} -point along the direction perpendicular to the 2D plane of the heterostructures. To avoid interactions between replicated images, a vacuum buffer of 20 Å was used. All the atomic positions in the systems were fully relaxed until the residual force were less than 0.001 eV/Å on each atom. Van der Waals (vdW) interactions were treated at the DFT-D3 level.^[52]

The relative stability of the different heterostructure studied can be estimated by means of their formation energy, E_f , calculated as:

$$E_f = E_{MoSSe/GaN} - E_{MoSSe} - E_{GaN} \quad (1)$$

$E_{MoSSe/GaN}$, E_{MoSSe} , and E_{GaN} are the total energy of the MoSSe/GaN heterostructure, and of the single-layer components (MoSSe and GaN) optimized in isolation, respectively. For the systems studied, the sign of E_f is negative in general as the systems pack via vdW interactions that are only attractive for a negligible interfacial relaxation. Thus, the more negative E_f , the larger the energetic favorability of the heterostructure.

The carrier mobility of the two-dimensional heterostructures can be calculated by the phonon-limited formula written as:^[53, 54]

$$\mu = (e\hbar^3 C_{2D}) / [k_b T m_e^* m_d (E_i)^2] \quad (2)$$

where m_e^* is the effective mass (m_x and m_y refer to the effective mass along the x and y direction), and $m_d^{e/h}$ is the equivalent density-of-state mass defined as $m_d = \sqrt{m_x m_y}$ (m_d^e for electron and m_d^h for the hole). E_i (i=e for the electron, i=h for the hole) is the deformation potential, calculated as $E_i = \Delta E_i / (\Delta L_i / L_i)$. E_i can be obtained from the band-energy change (ΔE_i) induced by a lattice compression or expansion of

step $\Delta L_i/L_i = 0.005$ in the transport direction. Based on this convention, the deformation potentials of one hole in the valence band maximum (VBM) and one electron in the conduction band minimum (CBM) are labelled as E_h , and E_e , respectively. The elastic moduli of the longitudinal acoustic C_{2D} in the propagation direction can be calculated as $C_{2D} = 2(E - E_0)/[S_0(\Delta L_i/L_i)^2]$, where E and E_0 are the total energy of the compressed/expanded and equilibrium geometries, respectively. S_0 is the area of two-dimensional material at the equilibrium geometry.

Results and Discussions

The Janus MoSSe system has a honeycomb hexagonal lattice with three atomic layers as shown in **Fig. 1(a)**. The optimized in plane lattice constant is $a=b=3.215$ Å, with Mo-S and Mo-Se bond lengths of 2.41 Å and 2.53 Å, respectively. Similar to Janus MoSSe, single layer Nitride GaN has also a hexagonal symmetry, as shown in **Fig. 1(b)**. Notably, the lattice constant of GaN is $a=b=3.26$ Å, only 0.045 Å larger than for MoSSe. Thus, an extremely small ratio of lattice mismatch at about $\sim 0.4\%$ can be achieved, when MoSSe and GaN form a heterostructure. Here, it should be noted that the basic structure parameters for single layer MoS₂ and MoSe₂ are also provided for the convenience to consider collocation effect in the following context.

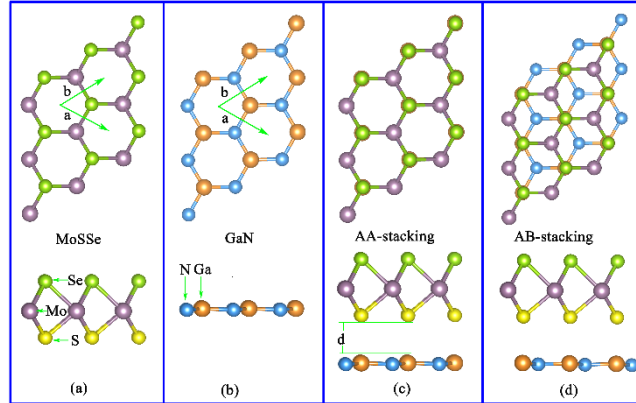


Figure 1. The atomic structure of single layer MoSSe (a), GaN (b), and their AA (c) and AB stacked (d) heterostructures. The top and side views are in the upper and lower panels, respectively. The primitive cell is marked by the green arrows. The Mo, S, Se, Ga, and N atoms are shown as light violet, yellow, light green, orange, and gray spheres, respectively. The letter “d” denotes the interlayer distance between the top and bottom layer.

Table 1. The basic structural parameters for the selected single layer TMDs and GaN. The lattice mismatch needed to form the heterostructure and the magnitude of band gap (E_g) are also shown. I and D indicate direct and indirect band gap (E_g), respectively.

System	Lattice $a=b$ (Å)	Length (Å)		Angle (°)		Ratio of mismatch	E_g (eV)
		Ga-N		$\angle \text{GaNGa}$			
		Mo-S	Mo-Se	$\angle \text{MoSMo}$	$\angle \text{MoSeMo}$		
GaN	3.250	1.87		120		0%	1.98(I)
MoSSe	3.215	2.41	2.53	83.73	79.09	0.4%	1.67(D)

MoS₂	3.152	2.403		81.97	1.2%	1.78(D)
MoSe₂	3.287		2.53	80.86	0.7%	1.54(D)

These results indicate that MoSSe and GaN can form vertical vdW heterostructures (MoSSe/GaN in the following) with minimal in-plane strain. Due to the different faces of MoSSe, two arrangements are possible for such heterostructures, which we refer to as SMoSe/GaN and SeMoS/GaN. In addition, for each arrangement the individual layers can be stacked according to either an AA or AB staking pattern, see **Fig. 1(c)** and **1(d)**. For the AA-stacked SeMoS/GaN, the S atom can sit above the Ga (denoted as AA-[S-Ga]) or the N atom (denoted as AA-[S-N]). More combinations become possible for AB-stacking. For the Mo atom of SMoSe/GaN sitting above the hollow-site of the GaN hexagonal lattice, there exist two kinds of possible AB-stacking depending on whether the Se atom sits above a Ga or N atom of the underlying GaN lattice. These structures are indicated as AB-[Se-Ga] or AB-[Se-N]. Conversely, for the Se atom of SMoSe/GaN sitting above the hollow-site of the GaN hexagonal lattice, two different AB-stacking are possible depending on whether the Mo atom sits on top of a Ga (AB-[Mo-Ga]) or N (AB-[Mo-N]) atom. In the following, the same labelling scheme is used also for the SeMoS/GaN heterostructure with S, not Se, atoms facing the underlying Ga/N layer.

Table 2. The calculated formation energy (E_f), interlayer distance (d), and band gap (E_g) for the considered MoSSe/GaN heterostructures in different (AA or AB) stacking. I and D in brackets denote indirect and direct band gap, respectively.

Mode	Stacking	Lattice (\AA)	E_f (eV)	d (\AA)	E_g (eV)
SeMoS /GaN	AA-[S-Ga]	3.234	-0.260	2.970	0.800(D)
	AA-[S-N]	3.233	-0.166	3.497	1.200(D)
	AB-[Mo-Ga]	3.236	-0.239	2.993	1.247(D)
	AB-[Mo-N]	3.234	-0.230	3.053	1.151(D)
	AB-[S-Ga]	3.239	-0.266	2.943	0.892(D)
SMoSe /GaN	AB-[S-N]	3.233	-0.163	3.523	1.185(D)
	AA-[Se-Ga]	3.237	-0.255	3.107	1.450(D)
	AA-[Se-N]	3.233	-0.227	3.22	1.517(D)
	AB-[Ga-Mo]	3.234	-0.236	3.226	1.631(D)
	AB-[Ga-N]	3.237	-0.230	3.053	1.150(D)
SMoS /GaN	AB-[Se-Ga]	3.238	-0.242	3.154	1.380(D)
	AB-[Se-N]	3.237	-0.167	3.592	1.616(D)
	AA-[S-Ga]	3.210	-0.212	2.988	0.767(D)
	AA-[S-N]	3.207	-0.121	3.036	1.134(D)
	AB-[Mo-Ga]	3.208	-0.19	3.036	1.221(D)
SMoS /GaN	AB-[Mo-N]	3.206	-0.184	3.103	1.127(D)
	AB-[S-Ga]	3.212	-0.209	2.967	0.837(D)
	AB-[S-N]	3.206	-0.118	3.526	1.117(D)
	AA-[Se-Ga]	3.265	-0.265	3.106	1.466(D)

/GaN	AA-[Se-N]	3.261	-0.172	3.573	1.557(D)
SeMoSe	AB-[Mo-Ga]	3.263	-0.237	3.119	1.531(D)
/GaN	AB-[Mo-N]	3.261	-0.241	3.169	1.590(D)
	AB-[Se-Ga]	3.266	-0.255	3.105	1.413(D)
	AB-[Se-N]	3.261	-0.170	3.609	1.540(I)

Table 2 reports the calculated formation energy, lattice constant, interlayer distance, and band gap of the different MoSSe/GaN heterostructures studied. The simulations indicate that AB-[S-Ga] stacking results in the lowest formation energy, E_f , of -0.266 eV in SeMoS/GaN, indicating this arrangement as the energetically favored. AA-[Se-Ga] stacking of the SMOSe/GaN heterostructure yields the second lowest E_f . Substitution of the upper MoSSe layer of the heterostructure with MoS₂ (SMoS) or MoSe₂ (SeMoSe) layers result in the AA-[S-Ga] (MoS₂/GaN) and AA-[Se-Ga] (MoSe₂/GaN) stacking being energetically favored with E_f of -0.212 eV and -0.265 eV, respectively. These results deviate from what previously calculated for heterostructures such as graphene and MoS₂ bilayers, for which AB-stacking is energetically favored. The results in Table 2 indicates also that E_f for the AB-[S/Se-Ga] stacking in general is comparable (to within XXX eV) to the AA-[S/Se-Ga] one, suggesting these patterns to be energetically competitive and potentially accessible by experiments.

The lower formation energy should origin from the different electron structure of the heterostructure. As for SMOs/GaN, S atoms for AA-[S-Ga] in negative valence attracts the Ga atoms in positive valence, resulting in stabilization of the heterostructure. Whereas the S atoms repels the N atoms in AA-[S-N] or other AB-stacking configurations and hence destabilizes the structures. This is consistent with the smaller interlayer distance in AA-[S-Ga]. Further, owing to the stronger oxidation of S atom than that of Se atom, the AA-[S-Ga] in SeMoS/GaN is about -0.01 eV lower than AA-[Se-Ga] in SMOSe/GaN. Therefore, the results show that AB-[S-Ga] is more stable in SeMoS/GaN, while AA-[S/Se-Ga] is always more stable than other stackings for other heterostructures.

Besides the structural stability and formation energy, we analyzed also the electronic properties of the heterostructures studies. The corresponding results in **Table 2** show that all the heterostructures studied are semiconductors regardless of the stacking type and relative atomic positions. The calculated band gap varies from 0.767 eV (SMoS/GaN, AA-[S-Ga]) to 1.631 eV (SMoSe/GaN, AB-[Ga-Mo]), which is located in the near visible-infrared region. Given the known underestimation errors the used PBE-GGA functional in calculating band-gap, these results suggest that visible light absorption for these systems may be possible. As also shown in **Table 2**, we find most of the heterostructures studied to have a direct band gas, in contrast with the indirect band gap for pristine GaN. Therefore, the simulations suggest that direct tuning of the electronic properties and, inevitably, light absorption of the heterostructures can be achieved by controlling the stacking geometry.

To further analyze the electronic properties of the lowest E_f heterostructures, we show their calculated band structure in **Fig. 2**. For all the systems, both the valence band maximum (VBM) and conduction band minimum (CBM) are located at the K point, suggesting that all these heterostructures are direct semiconductors. By changing the position of the S and Se atoms with respect to the underlying GaN layer, the band gap can vary from 0.77 to 1.47 eV. At the same time, as MoSSe changes to MoS₂, the energy level of K point is a little decreasing and CB in the range of Γ -K and Γ -M shifts upward as seen in **Fig. 2(e)**. But for the MoSe₂ case, the energy level of CB in Γ -K and Γ -M shifts downward see in **Fig. 2(g)**.

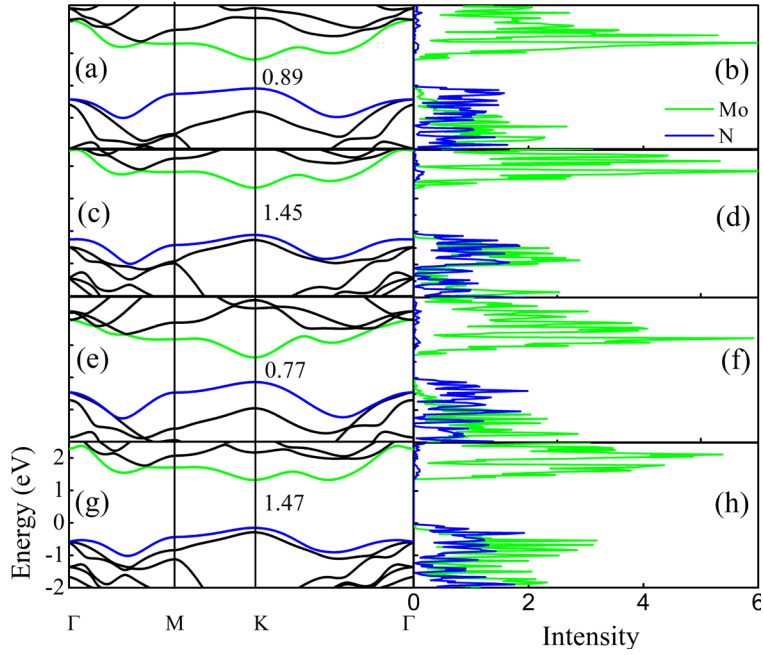


Figure 2. The calculated electron band structure and atom-projected density of states (PDOS) for the energy favored stacking of the MoSSe/GaN, MoS₂/GaN and MoSe₂/GaN heterostructure. (a-b) AB-[S-Ga] stacked SeMoS/GaN, (c-d) AA-[Se-Ga] stacked SMOSe/GaN, (d-e) AA-[S-Ga] stacked MoS₂/GaN, and (e-f) AA-[Se-Ga] stacked MoSe₂/GaN. The lowest and highest energy bands in the CB and VB are shown in green and blue, respectively. The Mo and N resolved PDOS are shown in green and blue, respectively.

To investigate the atomic contributions to VB and CB, **Fig. 2** reports also the calculated electron, atom-projected density of states (PDOS). For clarity, only the main contributions to the VBM and CBM are provided. The results indicate that, for all the systems, the main contribution to the VBM stem from the N_{2p} orbitals (blue line) of GaN. Conversely, the main contributions to the CBM are due to the Mo_{3d} orbitals (green line) of MoSSe, MoS₂ and MoSe₂. Therefore, the CBM and VBM are distributed on different side of the heterostructure. This result can be straightforwardly visualized by the band-decomposed charge densities for the VBM and CBM, shown for SMOSe/GaN as model system in **Fig. 3**. Evidently, whereas the CBM charge density for AA-[Se-Ga]

is mostly localized on the Mo atoms of the SMoSe layer, the VBM charge density is largest on the N atoms for the GaN layer. This intriguing property suggests that there is an intrinsic electronic field in the SMoSe/GaN heterostructure, which should be highly beneficial to separate photoinduced carriers.

The calculated dependence of the heterostructures' electronic properties on the stacking geometry prompts for investigation of its role for carrier mobility too. We start by benchmarking the accuracy of our approach to electron effective mass and mobility for single layer MoS₂ against previous results. We calculate an effective mass and carrier mobility of the electron in the CBM along X-K of 0.50 m_0 and 145.5 cm²V⁻¹s⁻¹, close to previously published result of 0.49 m_0 and 200 cm²V⁻¹s⁻¹[21].

Table 3 reports the calculated carriers effective and equivalent mass, deformation potential, electron and hole mobility for MoSSe/GaN, as well as MoS₂/GaN and MoSe₂/GaN in different stacking, together with results for single layer TMDs and GaN for comparison. For this analysis, we focus on the heterostructures with the lowest and second lowest E_f . Starting with MoSSe/GaN, the CBM electron mobility of AB-[S-Ga] stacked SeMoS/GaN along the X-K path is about 263.28 cm²V⁻¹s⁻¹, which is nearly three times larger than for single layer MoSSe (97.83 cm²V⁻¹s⁻¹). Conversely, the VBM hole mobility along the X-K path is about 3480.43 cm²V⁻¹s⁻¹, slightly smaller than for single layer GaN (3785.03 cm²V⁻¹s⁻¹). Qualitatively and quantitatively different results are computed for the other arrangements of the SMoSe/GaN heterostructure. The calculated electron and hole mobility of AA-[Se-Ga] are increased to 281.28 and 3951.21 cm²V⁻¹s⁻¹, respectively. These values are larger than for the isolated MoSSe and GaN layers. Therefore, the simulations indicate that the carrier mobility of MoSSe/GaN heterostructures can be substantially, up to nearly three times, larger than for the individual components.

Analysis of the carrier mobility can be extended by considering the role of S or Se exposure to GaN for calculated results. As the Se atom in MoSSe is substituted by S to form the MoS₂/GaN heterostructure, the electron mobility of AA-[S-Ga] decreases to 143.62 cm²V⁻¹s⁻¹. Also the hole mobility of AA-[S-Ga] stacked MoS₂/GaN decreases slightly (by 40.3 cm²V⁻¹s⁻¹) relative to the AA-[Se-GaN] stacking of MoSSe/GaN. In turn, as the S atom of MoSSe is changed into a Se atom to form MoSe₂/GaN heterostructure, the electron mobility becomes 258.25 cm²V⁻¹s⁻¹ similar to the value for SMoSe/GaN. In contrast, the hole mobility is strongly decreased by 3000 cm²V⁻¹s⁻¹. Thus, depending on the heterostructure composition, the carrier mobility can be tuned from 143.62 cm²V⁻¹s⁻¹ to 281.28 cm²V⁻¹s⁻¹ for the electron in the CBM, and from 791.34 cm²V⁻¹s⁻¹ to 3951.21 cm²V⁻¹s⁻¹ for hole in the VBM.

The simulations reveal an important role also of the heterostructure stacking for its carrier mobility. For instance, the electron and hole mobility of AA-[S-Ga] stacked SeMoS/GaN are about 13.82 and 1002 cm²V⁻¹s⁻¹ smaller than for the analogous AB-[S-Ga] stacked system. This trend is different from what shown by the other systems

studied, for which AA stacking is found to increase carrier mobility. Taking SMOSe/GaN as an example, the electron and hole mobility of AA-[Se-Ga] is increased by 8.38 and 259.06 $\text{cm}^2\text{V}^{-1}\text{s}^{-1}$ compared to AB-[Se-Ga]. Thus, we find that, depending on the AB or AA stacking, carrier mobility can be tuned by 19~123 $\text{cm}^2\text{V}^{-1}\text{s}^{-1}$ for electrons, and by 259~1002 $\text{cm}^2\text{V}^{-1}\text{s}^{-1}$ for holes. Comparing these results with the substantially larger compositional changes analyzed above, we are to conclude that carrier mobility in the considered heterostructures are substantially more sensitive to the occurrence of S/GaN or Se/GaN interfaces rather than AA or AB stacking.

Table 3. The calculated carrier mobility at 300 K for the (lowest and second lowest E_f) MoSSe/GaN, MoS₂/GaN, and MoSe₂/GaN heterostructures. The results for single layer Janus MoSSe, MoS₂, MoSe₂, and GaN are also provided for comparison. The $m_e^*/m_d^{e*}(m_o)$, $m_h^*/m_d^h(m_o)$, $E_e(E_h)(\text{eV})$, and $\mu_e(\mu_h)$ ($\text{cm}^2\text{V}^{-1}\text{s}^{-1}$) indicate the effective equivalent mass, deformation potential, carrier mobility for the electron at CBM (hole at VBM). C_{2D} ($\text{J}\cdot\text{m}^{-2}$) is the elastic moduli along the transport direction. It should be mentioned that only stable and next-stable configurations are considered.

System		m_e^*	m_d^e	m_h^*	m_d^h	E_e	E_h	C_{2D}	μ_e	μ_h
GaN		0.22	0.72	1.27	0.89	10.6	0.84	140.2	171.10	3785.03
MoS ₂		0.50	0.62	0.60	1.57	8.22	2.30	141.15	145.50	605.44
MoSSe		0.56	0.62	0.68	2.61	8.46	2.83	115.39	97.83	173.65
MoSe ₂		0.53	0.5	0.64	2.42	6.94	2.16	204.12	263.15	600.77
SeMoS	AA-[S-Ga]	0.53	0.66	1.49	1.06	8.0	1.20	264.10	249.46	2478.36
	/GaN AB-[S-Ga]	0.55	0.65	1.80	1.26	7.66	0.84	258.98	263.28	3480.43
SMoSe	AA-[Se-Ga]	0.54	0.7	1.23	1.45	7.47	0.91	275.5	281.28	3951.21
	/GaN AB-[Se-Ga]	0.52	0.70	1.82	0.84	7.62	1.00	266.86	272.90	3692.15
MoS ₂ /	AA-[S-Ga]	0.44	1.47	1.27	1.17	8.05	1.02	273.87	143.62	3910.91
	GaN AB-[S-Ga]	0.44	1.53	1.49	1.07	6.24	2.83	277.79	266.93	3050.20
MoSe ₂ /	AA-[Se-Ga]	0.73	0.69	1.39	1.14	6.66	2.16	271.91	258.25	791.34
GaN	AB-[Se-Ga]	0.61	0.68	1.00	0.99	8.41	1.81	265.58	191.53	1739.03

In order to identify the origin of diverse carrier mobility in heterostructures studied, we systemically calculated the effective and equivalent mass, deformation potential, and elastic moduli as shown in **Table 3**. Identification of the crucial factor(s) behind the carrier mobility is essential for definition of synthetic strategies to enhance it. Taking AA-[Se-Ga] stacked SMOSe/GaN as case study, the electron mobility is about two times that of MoSSe, and the hole mobility is close to isolated GaN layer. However, the effective mass, equivalent mass, deformation potential, and elastic moduli of the electron (hole) are about 0.98 (0.97), 1.13 (1.63), 0.88/1.08, and 2.4/1.96 times larger, while the carrier mobility are about 1.94/1.05 times larger than that of single layer SMOSe (GaN). According to Eq. (2), effective (equivalent) mass and deformation potential are inversely proportional, while the elastic modulus is linearly proportional

to the carrier mobility. Clearly, the electron carrier mobility is mainly determined by the elastic moduli, while the hole carrier mobility is also related to equivalent mass and elastic moduli. The case for AA-[S-Ga] of MoS₂/GaN is different. The effective mass, equivalent mass, deformation potential, and elastic moduli of the electron (hole) are about 0.88 (1.00), 2.37 (1.31), 0.98 (1.21), and 1.94 (1.94) times larger than that of single layer MoS₂ (GaN), while the carrier mobility of electron (hole) is about 0.99 (1.03) times. The electron carrier mobility is mainly determined by the equivalent mass and elastic moduli, while the hole carrier mobility is also related to deformation potential.

The above results indicate that both electron and hole carrier mobility are affected by equivalent mass and elastic moduli. Thus, equivalent mass and elastic moduli should be the main factors on determining the carrier mobility during forming heterostructure from single component. The larger elastic moduli origins from the thicker thickness of heterostructure compared with those of its single component. As for the larger equivalent mass, it can be related to the extremely flat character of the CMB along the Γ -M path (**Fig. 2**)

Then, it is interesting to know the reason why electron and hole behaves markedly differently. As for SMoSe/GaN, the electron mobility of AA-[Se-Ga] is 281.28 cm²V⁻¹s⁻¹, while the hole mobility is 3951.21 cm²V⁻¹s⁻¹ about 14 times larger than for the electron. The ratio of effective mass, equivalent mass, deformation potential, and elastic moduli between hole and electron are about 2.23, 2.1, 0.12, and 1.0. Accordingly, we are to infer that the deformation potential should be the dominant factor. The different deformation potential can be seen from the different bonding characteristic of valence band and conduction band. For the electron in CBM, the charge distribution is mainly localized in the x - y plane in Mo_{3d} orbitals (see **Fig. 3(c)**), which is larger than the distribution of VBM with the electron localized only at N_{2p} orbitals (see in **Fig. 3(d)**). As structural deformation occurs, it will generate stronger electrostatic interaction in CBM than that in VBM, corresponding to larger E_e than E_h . Therefore, smaller deformation potential contributes to larger hole carrier mobility for the heterostructure.

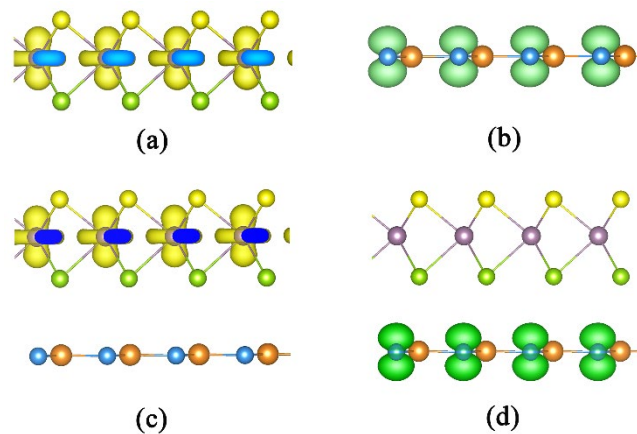


Figure 3. (Color online) (a)-(b) Side views of the density-distribution of the CBM in

SMoSe (a) and of the VBM in GaN (b). (c)-(d) The side view of density-distribution of the the CBM and the VBM for the MoSSe bilayer. The isovalue for the contour plot is $0.01 e \text{ bohr}^{-3}$.

As discussed above, the electron and hole carrier mobility can also be influenced by stacking of the heterostructure. As for stacking effect, the result indicates that the carrier mobility of second lowest E_f structure is always smaller than for the lowest E_f stacking. This difference should origin from a slight larger equivalent mass and deformation potential of the distinct atoms. However, as for the collocation effect, it can be found that no clear tendency can be from as the collocation of changing S (Se) of MoSSe to Se (S) atom.

Conclusion

In summary, the structural, electronic and carrier mobility properties of MoSSe/GaN heterostructures are systematically investigated by the first-principles calculations. It shows that Janus MoSSe/GaN heterostructure has a relatively high carrier mobility of $281.28 \text{ cm}^2\text{V}^{-1}\text{s}^{-1}$ for electron and $3951.2 \text{ cm}^2\text{V}^{-1}\text{s}^{-1}$ for hole. Except the intrinsic electric field of Janus MoSSe, the carrier mobility can be further regulated through the different stacking strategies and Janus atomic structure of MoSSe. The results further indicates that the superior carrier mobility of Janus MoSSe/GaN heterostructure are affected by the equivalent mass and elastic moduli. These results showed that the Janus MoSSe/GaN heterostructure has a potential to be used as electronic device for their carrier mobility.

Acknowledgements

This work was supported by the Science Challenge Project (TZ2018004), the National Natural Science Foundation of China (Nos. 51572016, U1530401, 11747167, 11804090, 51472209, 11774298, U1401241, and 21503012), the Natural Science Foundation of Hunan Province, China (Grant No. 17C0626, and 2019JJ50148), and the Scientific Research Fund of University (No. E517558). This research was also supported by a Tianhe-2JK computing time award at the Beijing Computational Science Research Center (CSRC). L.M.L. and G. T. acknowledge also support by the Royal Society Newton Advanced Fellowship scheme (grant No. NAF\R1\180242).

References

- [1] Y. Gao, T. Cao, F. Cellini, C. Berger, W. A. de Heer, E. Tosatti, E. Riedo, and A. Bongiorno, *Nat Nanotechnol* **13**, 133 (2018).
- [2] C. Tan, et al., *Chem. Rev.* **117**, 6225 (2017).
- [3] W.-J. Yin, B. Wen, C. Zhou, A. Selloni, and L.-M. Liu, *Surface Science Reports* **73**, 58 (2018).
- [4] Y. Zhang, Y.-W. Tan, H. L. Stormer, and P. Kim, *Nature* **438**, 201 (2005).
- [5] K. S. Novoselov, A. K. Geim, S. V. Morozov, D. Jiang, M. I. Katsnelson, I. V. Grigorieva, S. V. Dubonos, and A. A. Firsov, *Nature* **438**, 197 (2005).
- [6] M. Wang, Y. Pang, D. Y. Liu, S. H. Zheng, and Q. L. Song, *Computational Materials Science* **146**, 240 (2018).
- [7] A. K. Geim, *Science* **324**, 1530 (2009).

- [8] K. S. Novoselov, A. K. Geim, S. V. Morozov, D. Jiang, Y. Zhang, S. V. Dubonos, I. V. Grigorieva, and A. A. Firsov, *Science* **306**, 666 (2004).
- [9] C. Lin, D. Shin, and A. A. Demkov, *Journal of Applied Physics* **117**, 225703 (2015).
- [10] Z.-K. Han, Y.-Z. Yang, B. Zhu, M. V. Ganduglia-Pirovano, and Y. Gao, *Physical Review Materials* **2** (2018).
- [11] T. Umebayashi, T. Yamaki, H. Itoh, and K. Asai, *Journal of Physics and Chemistry of Solids* **63**, 1909 (2002).
- [12] H. C. Yang, Y. Xie, J. Hou, A. K. Cheetham, V. Chen, and S. B. Darling, *Adv Mater* **30**, e1801495 (2018).
- [13] Y. Gong, et al., *Nature Nanotechnology* (2018).
- [14] Y.-N. Z. Hui Zhang, Hao Liu and Li-Min Liu, *J. Mater. Chem. A* **2**, 15389 (2014).
- [15] M. Chhowalla, H. S. Shin, G. Eda, L.-J. Li, K. P. Loh, and H. Zhang, *Nat Chem* **5**, 263 (2013).
- [16] C. Ataca, H. Şahin, and S. Ciraci, *The Journal of Physical Chemistry C* **116**, 8983 (2012).
- [17] Q. Xiang, J. Yu, and M. Jaroniec, *Journal of the American Chemical Society* **134**, 6575 (2012).
- [18] B. Radisavljevic and A. Kis, *Nature materials* **12**, 815 (2013).
- [19] W. S. Yun, S. W. Han, S. C. Hong, I. G. Kim, and J. D. Lee, *Physical Review B* **85** (2012).
- [20] S. Fathipour, et al., *Applied Physics Letters* **105**, 192101 (2014).
- [21] RadisavljevicB, RadenovicA, BrivioJ, GiacomettiV, and KisA, *Nat Nano* **6**, 147 (2011).
- [22] G. Mattioli, F. Filippone, P. Alippi, and A. Amore Bonapasta, *Physical Review B* **78** (2008).
- [23] S. Najmaei, et al., *Nature materials* **12**, 754 (2013).
- [24] X. Ma, X. Wu, H. Wang, and Y. Wang, *Journal of Materials Chemistry A* **6**, 2295 (2018).
- [25] R. Chaurasiya and A. Dixit, *Applied Surface Science* **490**, 204 (2019).
- [26] Y. Cai, G. Zhang, and Y. W. Zhang, *Journal of the American Chemical Society* **136**, 6269 (2014).
- [27] A.-Y. Lu, et al., *Nature Nanotechnology* **12**, 744 (2017).
- [28] J. Zhang, et al., *ACS nano* **11**, 8192 (2017).
- [29] R. Peng, Y. Ma, S. Zhang, B. Huang, and Y. Dai, *The journal of physical chemistry letters* **9**, 3612 (2018).
- [30] W. Chen, E. J. Santos, W. Zhu, E. Kaxiras, and Z. Zhang, *Nano letters* **13**, 509 (2013).
- [31] K. F. Mak, C. Lee, J. Hone, J. Shan, and T. F. Heinz, *Physical Review Letters* **105**, 136805 (2010).
- [32] S. Cahangirov, C. Ataca, M. Topsakal, H. Sahin, and S. Ciraci, *Physical Review Letters* **108**, 126103 (2012).
- [33] W.-J. Yin, B. Wen, G.-Z. Nie, X.-L. Wei, and L.-M. Liu, *Journal of Materials Chemistry C* **6**, 1693 (2018).
- [34] H. C. Yang, J. Hou, V. Chen, and Z. K. Xu, *Angew Chem Int Ed Engl* **55**, 13398 (2016).
- [35] H. L. Wang, L. S. Zhang, Z. G. Chen, J. Q. Hu, S. J. Li, Z. H. Wang, J. S. Liu, and X. C. Wang, *Chem. Soc. Rev.* **43**, 5234 (2014).
- [36] Y.-m. Ding, et al., *Nanoscale* **9**, 14682 (2017).
- [37] F.-B. Zheng, L. Zhang, J. Zhang, P.-j. Wang, and C.-W. Zhang, *Physical Chemistry Chemical Physics* **22**, 5163 (2020).
- [38] J. C. Yongsheng Yao, Wenjin Yin, Liwen Yang and a. X. Wei, *J. Phys. D: Appl. Phys.* **53** (2020).
- [39] W. Li, Z. Lin, and G. Yang, *Nanoscale* **9**, 18290 (2017).
- [40] X. Sun, H. Deng, W. Zhu, Z. Yu, C. Wu, and Y. Xie, *Angew Chem Int Ed Engl* **55**, 1704 (2016).
- [41] Z. Wei, F. F. Liang, Y. F. Liu, W. J. Luo, J. Wang, W. Q. Yao, and Y. F. Zhu, *Appl. Catal. B-Environ.* **201**, 600 (2017).

- [42] W. Yin, B. Wen, Q. Ge, D. Zou, Y. Xu, M. Liu, X. Wei, M. Chen, and X. Fan, *Progress in Natural Science: Materials International* **29**, 335 (2019).
- [43] W. Yin, B. Wen, Q. Ge, X. Wei, G. Teobaldi, and L. Liu, *Progress in Natural Science: Materials International* **30**, 128 (2020).
- [44] M. L. Sun, J. P. Chou, Q. Q. Ren, Y. M. Zhao, J. Yu, and W. C. Tang, *Appl. Phys. Lett.* **110**, 173105 (2017).
- [45] Z. L. Lu, D. Y. Zhi, G. Jing, C. R. Ze, X. Y. Zong, and L. Wei, *Mater. Lett.* **213**, 387 (2018).
- [46] Zakaria Y. Al Balushi¹, KeWang³, Ram Krishna Ghosh^{4,5}, Rafael A. Vilá^{1,2}, Sarah M. Eichfeld^{1,2,3}, X. Q. Joshua D. Caldwell⁶, Yu-Chuan Lin^{1,2}, Paul A. DeSario⁶, Greg Stone^{1,3}, Shruti Subramanian¹, Dennis F. Paul⁸, Robert M. Wallace⁷, Suman Datta^{4,5}, Joan M. Redwing^{1,2,3,5}, and Joshua A. Robinson^{1, 3}, *Nature materials* (2016).
- [47] Y. Zhao, H. Wang, H. Zhou, and T. Lin, *Small* **13** (2017).
- [48] X. Li, Z. Li, and J. Yang, *Physical review letters* **112**, 018301 (2014).
- [49] G. Kresse and J. Hafner, *Physical Review B* **47**, 558 (1993).
- [50] G. K. a. J. Furthmuler, *Physical Review B* **54**, 11169 (1996).
- [51] J. Heyd, G. E. Scuseria, and M. Ernzerhof, *The Journal of Chemical Physics* **124**, 219906 (2006).
- [52] S. Grimme, J. Antony, S. Ehrlich, and H. Krieg, *J. Chem. Phys.* **132**, 154104(1) (2010).
- [53] X.-B. Li, P. Guo, Y.-N. Zhang, R.-F. Peng, H. Zhang, and L.-M. Liu, *Journal of Materials Chemistry C* **3**, 6284 (2015).
- [54] S. Bruzzone and G. Fiori, *Applied Physics Letters* **99**, 222108 (2011).